Nanoscale

PAPER

View Article Online
View Journal

Cite this: DOI: 10.1039/c8nr04038a

Natural killer cells' immune response requires a minimal nanoscale distribution of activating antigens†

Yossi Keydar,[a,b] Guillaume Le Saux,[a,b] Ashish Pandey,[a,b] Edri Avishay,[c] Netanel Bar-Hanin,[a,b] Toledo Esti,[a,b] Viraj Bhingardive,[a,b] Uzi Hadad,[b] Angel Porgador[c] and Mark Schvartzman *[a,b]

NK cells recognize cancer and viral cells by binding their activating receptors to antigens presenting on the membrane of target cells. Although the activation mechanism of NK cells is a subject of extensive research today, the role of the composition and spatial distribution of activating ligands in NK cell cytotoxicity is barely understood. In this work, we engineered a nanochip whose surface was patterned with matrices of antigens for NKG2D activating receptors. These matrices mimicked the spatial order of the surface of antigen presenting cells with molecular resolution. Using this chip, we elucidated the effect of the antigen spatial distribution on the NK cell spreading and immune activation. We found that the spatial distribution of the ligand within the 100 nm length-scale provides the minimal conditions for NKG2D regulated cell spreading. Furthermore, we found that the immune activation of NK cells requires the same minimal spatial distribution of activating ligands. Above this threshold, both spreading and activation plateaued, confirming that these two cell functions work hand in hand. Our study provides an important insight on the spatial mechanism of the cytotoxic activity of NK cells. This insight opens the way to rationally designed antitumor therapies that harness NK cytotoxicity.

Received 18th May 2018,
Accepted 11th July 2018

DOI: 10.1039/c8nr04038a

rsc.li/nanoscale

Natural killer (NK) cells are large granular lymphocytes able to eliminate cancer and viral cells.[1–3] NK cells play the key role in the innate immune system by providing the first line of defense against viruses, as was clearly shown by the strong infections in humans and mice lacking NK cells.[4,5] NK cells have the ability to distinguish between healthy and diseased cells, and directly attack tumor, virus-infected, or stressed cells.[6] In healthy human adults, between 5% to 15% of peripheral blood lymphocytes belong to the family of NK cells,[7] most of which (~90%) are $CD56^{dim}$ $CD16^{bright}$ that provide a strong cytolytic response, and about 10% are $CD56^{bright}CD16^{null/dim}$ capable of fast cytokine secretion.[8]

The cytotoxicity of NK cells is regulated by activating and inhibitory receptors, whose signaling balance determines whether a target cell will be tolerated or attacked. The detection of a target cell by the NK cell is followed by the formation of natural killer immune synapse (NKIS) – a delicately regulated molecular cluster at the interface between the two cells.[9,10] The main function of lytic NK immune synapse is to allow the secretion of lytic granules that contain granzymes – lytic effector molecules, which induce programmed death in the target cells and eliminate them.[9] Notably, NK cells do not express variable antigen specific receptors. Instead, their function is regulated by a multitude of germ-line encoded activating and inhibitory receptors that recognize different cognate ligands expressed by target cells.

NK cell cytotoxicity is a highly controlled process that involves NK cell adhesion to target cells, and the interaction between activating NK cell receptors and their respective ligands on the target cell surface. Among different activating receptors in NK cells, the C-type lectin-like receptor NKG2D is known to play a key role in NK cell activation and its important functions such as tumor recognition.[11] NKG2D is a type II transmembrane glycoprotein, which, in addition to NK cells, is also expressed on the membrane of $CD8^+$ T cells.[12] Ligands for human and murine NKG2D include human MICA/B, and ULBPs ligands, as well as the mouse H60, Mult1 and the Rae-1 family.[13–16] These ligands are largely expressed on tumor

[a]Department of Materials Engineering, Ben Gurion University of the Negev, Beer Sheva 84105, Israel. E-mail: marksc@bgu.ac.il
[b]Ilse Katz Institute for Nanoscale Science & Technology, Ben Gurion University of the Negev, Beer Sheva 84105, Israel
[c]The Shraga Segal Department of Microbiology, Immunology and Genetics, Faculty of Health Sciences, Ben Gurion University of the Negev, Beer Sheva 84105, Israel

†Electronic supplementary information (ESI) available. See DOI: 10.1039/c8nr04038a

cells,[17–19] whereas each of them has its own expression pattern depending on the ligand function and tumor type.[20,21] For instance, MICA ligands are often discovered on epithelial tumors, yet rarely on hematological malignancies. In addition, NKG2D ligands are upregulated on virus-infected cells. For instance, MICA was found to be highly expressed in epithelial cells following infection with adherent *Escherichia Coli*,[22] as well as on endothelial cells and fibroblasts infected with cytomegalovirus.[23] Finally, MIC ligands are upregulated on activated immune cells, such as dendritic cells stimulated with interferon (IFN)-α,[24] and macrophages activated by Lipopolysaccharides.[25] Such a high expression of NKG2D ligands, in particular those of the MIC family, triggers NKG2D-mediated NK cell cytotoxicity. Yet, although not commonly, ligands for NKG2D can be also expressed in healthy tissues. Both MICA and MICB were found to be present on the membrane of normal intestinal epithelial cells, most probably due to stimulation of bacterial flora in the gut.[26] Recent reports showed a broad expression of MICA and MICB within normal epithelial cells, with a small fraction appearing on the cell surface.[27]

Since the cytotoxicity of NK cells is managed by the signaling balance of activating, costimulatory, and inhibitory receptors, the repertoire of different ligands expressed on the membrane of target cell determines whether it will be attacked or tolerated.[28–31] Yet, given the different levels of expression of NK activating ligands on infected, transformed, and activated immune cells, as well as on several healthy cells, it is reasonable to hypothesize that the level of expression of activating ligands regulates cytotoxic activity of NK cells, and that there could be minimal requirements for the expression of activating ligands to stimulate the cytotoxic response of NK cells. To elucidate these requirements, signals induced by activating ligands must be isolated and studied independently of costimulatory and inhibitory signaling. Such a study requires, in turn, systematic and controlled variation of the composition and spatial distribution of the activated ligands, together with monitoring of the effect of this variation to the immune activity.

Here, we investigated *in vitro* how the activation and cytotoxic activity of NK cells is regulated by the spatial distribution of MICA ligands in the membrane of the target cell. For this purpose, we activated human NK cells on a nanochip, whose surface is patterned with systematically varied nanopatterned matrices of MICA ligands (Fig. 1). Thus, the chip surface functions as an "artificial APC membrane" that activates NK cells, in which the ligand nanopattern deterministically encodes the spatial arrangement of formed NKG2D-MICA pairs. To simultaneously monitor how NK cells react to different activation conditions, we engineered the chip with multiple matrices that were designed with systematically tuned nanoscale periodicities. Each matrix on the chip was intended to provide an isolated microenvironment for NK cell activation, in which the MICA spatial distribution is regulated independently from other matrices.

Importantly, the size of NKG2D-MICA complex is about 10 nm.[32] Therefore, clustering of individual NKG2D receptors within the cell membrane be regulated by anchoring them to the ligand domains of 10 nm or smaller. To enable such delicate positioning of ligands, we immobilized them onto nanopatterned metallic nanodots sized around 10 nm, thereby creating synthetic vacancies for the recognition by discrete transmembrane receptors.[33–35] We fabricated the nanodots by the previously reported by us approach that combines nanoimprint lithography and angle-evaporation metal mask, which could produce arbitrary designed arrays metallic features sized down to 3.5 nm.[36] We designed the with orthogonal nanodot matrices, whose 2D unit cell was varied between 50 nm to 200 nm. Notably, this length scale fits the recently reported spatial organization of activating and inhibitory receptors in NK cells.[37] We functionalized the nanodots *via* thiols terminated with Ni-chelated nitrilotriacetic acid (NTA), to which we attached of histidine-conjugated MICA molecules.[38] We verified the selectivity of our functionalization by immunofluorescent staining of immobilized MICA with fluorophore-conjugated antibody, followed by the fluorescent imaging on the arrays on the chip. Using our biochips, we then monitored the activation of NK cell in several microenvironments, which were different from each other by spatial distribution of MICA. We found that the average area of the spread NK cell was dependent on the density of MICA, and that the surface density of 100 ligated nanodots per square micron was the threshold for NK cell spreading. Furthermore, we assessed the degree of NK cell activation by fluorescent imaging of lysosomal-associated membrane protein CD107, which is a commonly used functional marker for NK cell cytotoxic activity. We found, that whereas MICA density barely influences the average amount of CD107a per cell, it regulates the average probability of whether a cell will be activated or not, and exhibits exactly the same dependence on MICA spatial distribution as does spreading.

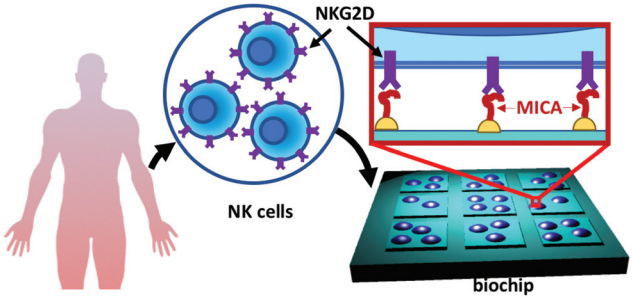

Fig. 1 Schematic presentation of the chip for the control the spatial distribution of NKG2D receptors in NK cells.

Experimental details

Nanochip fabrication

The fabrication and functionalization scheme is briefly descried in Fig. 2. We based the chip fabrication on our previous report based on nanoimprint lithography.[34,36] First, we produced a nanoimprint mold using electron beam lithography of hydrogen silsesquioxane (HSQ, XR-1541, Dow Corning).

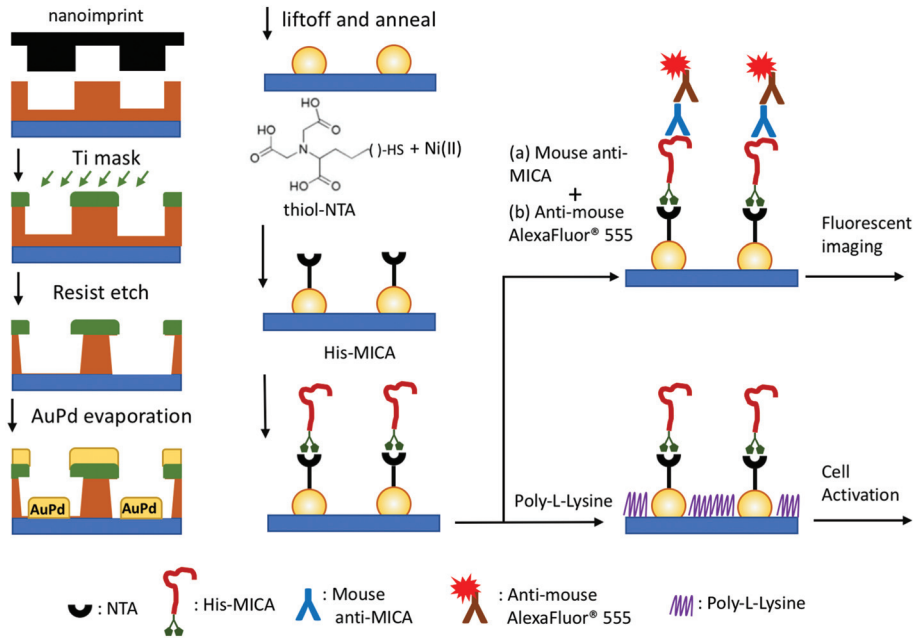

Fig. 2 Schematic process flows of the fabrication of AuPd nanodots by nanoimprint lithography, their functionalization with MICA, and MICA immunofluorescent labeling.

To that end, we diluted HSQ in Methyl Isobutyl Ketone (MIBK) and spin-coated it on a silicon substrate to produce a 20 nm thick film. We patterned the HSQ film using Raith e-LINE with an acceleration voltage of 20 kV, aperture of 30 μm and working distance of 10 mm, and developed in 0.26 N TMAH solution (AZ726, Rohm and Hass) for 2 min, following DI water rinsing and drying with nitrogen. We then annealed the mold at 450 °C for 1 hour, and coated it with an anti-adhesive monolayer (NXT-110, Nanonex NXT-110).

We produced the nanochips on either glass coverslips or silicon substrates. We first spin-coated PMMA (50 K, Microchem) diluted in anisole onto the substrates, and baked them on a hot plate heater to 180 °C for 2 min. The PMMA thickness was 40 nm. We imprinted PMMA using a commercial nanoimprint tool (NX-B100, Nanonex), with the following parameters: pressure of 450 psi, temperature of 180 °C, and an imprinting time of 4 minutes. We then evaporated a Ti mask of ~15 nm on top of the imprinted PMMA film, while tilting the sample at 30° to ensure that the mask covers the top PMMA surface but not the bottom of the imprinted features. We etched PMMA through the formed Ti mask with oxygen plasma (Corial 200 IL, plasma conditions), and evaporated a film of Ti/AuPd (1 nm/3 nm) perpendicularly to the chip surface. Finally, we performed liftoff of PMMA by immersing the chips in boiling acetone, and shrunk the formed nanodots by thermal annealing for 1 hour at 550 °C under N_2 atmosphere.

Chip biofunctionalization by the ligand immobilization

First, we cleaned the chips with ethanol and water, respectively, then dried them under a stream of nitrogen, baked at 120 °C for 5 min, and cleaned with oxygen plasma (Harrick PDC-32G, 1 min). Then, we immersed the chips overnight into a 0.2 mM ethanoic solution of thiol-NTA (NTA terminal-SAM formation reagent, Sigma-Aldrich). After generous rinsing with ethanol and water respectively, we chelated the NTA with Nickel by incubating the chips in nickel(II) chloride hexahydrate (0.5 M) for two hours, followed by rinsing in water. We then incubated the chips overnight at 4 °C in a 2 μg mL^{-1} solution of His-MICA (SinoBiological) in Phosphorous Buffer Solution (PBS), and rinsed the chips twice by immersing them for 5 min in PBS with 0.1% Tween20, and once with net PBS. Finally, we incubated the samples for 5 min in 0.01% w/v solution of poly-l-lysine in water, rinsed twice with PBS, and stored in PBS before being used for cell studies.

Immunofluorescence characterization

MICA modified surfaces were blocked for 30 min at 37 °C in PBS with 5% w/v skim milk. Samples were then incubated overnight at 4 °C with anti-MICA antibody (Abcam) at a concentration of 1 μg mL^{-1} in PBS with 5% skim milk, followed by rinsing 3 × 5 min in PBS with 0.2% Tween20. Then, surfaces were incubated 1 hour at 37 °C in a 1 : 500 solution of anti-Mouse Alexa 568 (Life Technologies) in PBS with 5% skim milk. Finally, samples were rinsed 3 × 5 min in PBS with 0.2% Tween20 followed by one rinse in pure water and mounted on a coverslip with DAKO Fluorescence Mounting Medium (Agilent).

Primary NK cell purification and propagation

We purified primary NK (pNK) cells from peripheral blood of a healthy and adult volunteer donor, recruited by written

informed consent, as approved by the Institutional Review Board Ben-Gurion University of the Negev (BGU). We isolated the cells using a human negative selection based NK isolation kit (RosetteSep, Miltenyi Biotec). We then cultured the purified NK cells in stem cell serum-free growth medium (CellGenix GMP SCGM, 20802-0500) supplemented with 10% heat-inactivated human AB plasma from healthy donors (SIGMA, male AB, H-4522), 1% L-glutamine, 1% Pen-Strep, 1% sodium pyruvate, 1% MEM-Eagle, 1% HEPES 1 M, and 300 IU mL^{-1} recombinant human IL-2 (PeproTech).

NK cell activation on the chip

We seeded the cultured pNK cells onto the chip surface in growth medium containing <2% serum and 50 units of IL-2, and left them to adhere for 3–4 hours. We then rinsed twice the surfaces in PBS to remove non-adherent cells, and fixed adherent cells with 4% PFA, permeabilized them with 0.5% Triton-X 100, and blocked with 5% skim milk in PBS. We stained the actin cytoskeleton with Alexa Fluor® 555 phalloidin, and the cell nuclei by mounting the samples with ProLong® Gold antifade reagent containing DAPI (Both from Life Technologies).

For the imaging of CD107a (the degranulation marker), we seeded the cultured pNK cells as previously mentioned, using medium supplemented with APC anti-human CD107a (1 : 1000 v/v), and left them to adhere 3 hours. We then renewed the medium and placed (6 well plates with cells) on ice for 30 min to maximize membrane bound CD107a. We rinsed the chip surface twice in PBS, fixed the cells with 4% PFA, and then directly stained with Alexa Fluor® 555 phalloidin without permeabilization to prevent damage to the cell membrane. Finally, we stained the nuclei by mounting the samples with ProLong® Gold antifade reagent containing DAPI.

Microscopy

We imaged the fluorescently labeled chip surface, as well as the cells activated in the cup, using Zeiss LSM880 confocal microscope, and quantified the obtained images using Fiji imaging software (https://fiji.sc). For APC anti-CD107a quantification of fluorescence intensity, exposure time, detector gain, and laser power were optimized once on the first sample and then locked. From the APC anti-CD107a signal, we quantified the percentage of activated cells by applying a threshold below which cells were considered non-activated.

Results

Chip fabrication and biofunctionalization

We fabricated the chips using both silicon substrates and glass coverslips. Each matrix was 400 × 400 microns in size, and was able to contain about 90 incontiguous cells. We used Silicon chips for the imaging of the nanodot arrays with scanning electron microscope (SEM) (Fig. 3a–d), and verified that the dot size in each matrix was 8–10 nm (Fig. 3e and f). We also used glass chips for the fluorescent microscopy of biofunctionalized and immunoassayed ligand matrices, as well as for the imaging of activated cells. To verify the selectivity and specificity of our functionalization scheme, we immunostained MICA immobilized onto the nanodots with mouse anti-MICA antibody and anti-mouse antibody labeled with Alexafluor 568 tag. We could not image individual functionalized dots, since the distance between the dots was below the resolution limit of an optical microscope, but we still could clearly see the fluorescent image coming for the whole nanopatterned areas (Fig. 3a–d, insets). Importantly, a low signal coming from the glass background indicates that possible unspecific immobilization of MICA to glass is negligible.

To further investigate the nature of the MICA immobilization of the metallic nanopattern using NTA/Ni-HIS based conjugation, we quantified the fluorescent signal coming from different matrices, and checked a possible correlation between the signal intensity and the dot density. Indeed, we found nearly linear dependence of the fluorescent signal on the nanodot density, indicating that nearly the same average

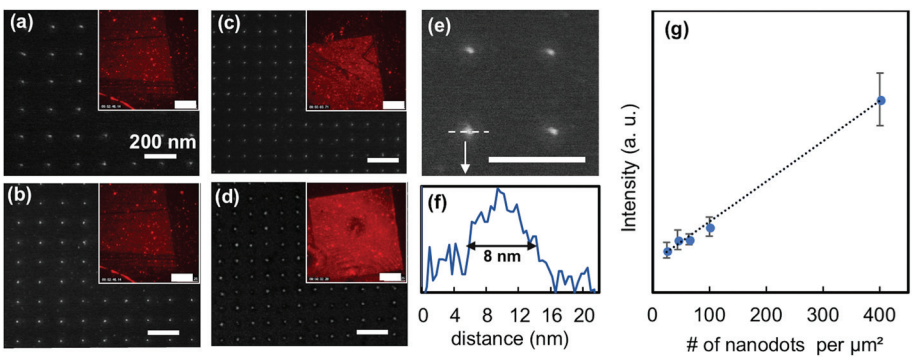

Fig. 3 Chip fabrication and functionalization. (a)-(d) – SEM images of nanodot in different matrices with the periodicity of 200 nm, 150 nm, 100 nm, and 50 nm, receptively. Scale bar: 200 nm. Insets: Florescent image of the matrices functionalized wit MICA and immunostained with Alexafluor 555 tagged antibody. Scale bar in insets: 50 microns. (e) High magnification SEM of nanodots. Scale bar: 100 nm. (f) Color profile of a single nanodot, with the full-width half-maximum of 8 nm. (g) Intensity of the fluorescence signal obtained from the matrices *vs.* the nanodot density.

number of MICA molecules and antibodies are immobilized per nanodot in each matrix (Fig. 3g).

NK cell spreading

To assess the sensitivity of NK cells to the spatial distribution of MICA ligands, we first estimated the average cell area on different matrices of the chips. Importantly, in addition to the nanopatterns of ligands, our chip contained plain AuPd areas produced by the mechanical removal of the resist outside the nanopatterned region right before the deposition of AuPd. We assumed that MICA was immobilized on this area in closely packed monolayer. We used plain AuPd and bare glass areas as upper and lower limits of MICA density, respectively.

In the cell spreading experiments, we incubated the NK cells on the chip surface for 3 hours before fixation (Fig. 4a and b). Importantly, we found that immobilizing poly-L-lysine onto the areas is critical to facilitate cell adhesion to the surface. Three hours is a suffice time for activated NK cells to enhance CD107a expression on the cell membrane following lytic vesicles release.[39] Fig. 4c presents the average projected area of NK cells *vs.* the density of the MICA functionalized dots. Two regions are clearly seen in the plot. In the areas with no MICA, as well as in the areas with MICA densities of 26 and 44 MICA-ligated nanodots per square micron, which correspond to the matrices with unit cells of 200 and 150 nm, respectively, the average projected area was about 60 square microns – the same as of suspended cells (see ESI†). Therefore, the cells did not spread on these areas. The density of 100 dots per square microns, which corresponds to the unit cell of 100 nm, is a threshold, above which the NK cells spread over the area three time higher compared to the non-spread cells. Interestingly, above this threshold density, the cells reached a plateau in their average area.

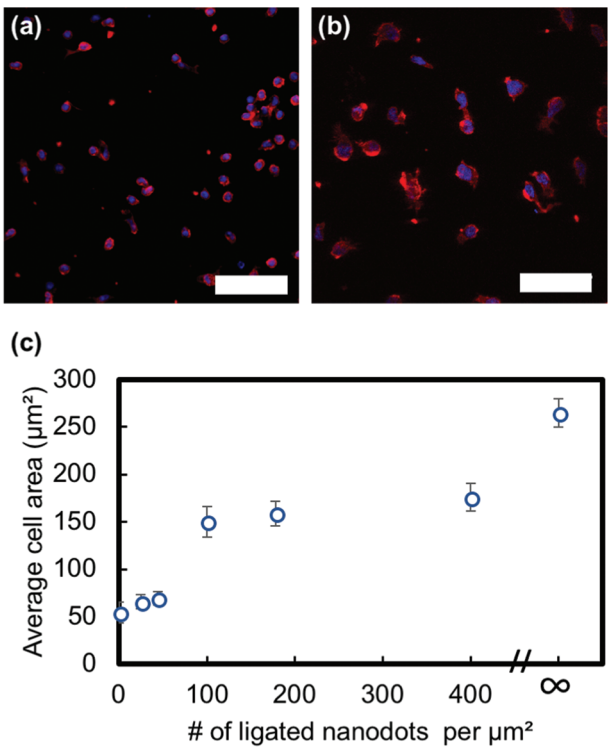

Fig. 4 NK cell spreading. (a) and (b) NK cells after 3 hours of activation on the matrices with 50 nanodots per μm^2 and 400 nanodots per μm^2, respectively. The cells were stained for cytoskeleton (red), nuclei (blue). Scale bars: 50 μm. (c) Average area projected by cells *vs.* nanodot density. Here ∞ means continues AuPd layer functionalized with MICA, providing the maximal ligand density.

Percentage of activated NK cells is regulated by the ligand density

To further investigate the influence of ligand density on the cytotoxic activity of NK cells, we imaged and quantified the expression of CD107a.[40,41] CD107a is used as a marker for the immune function of NK cells, since activated NK cells transport lytic granules to the immune synapse and fuse them to the membrane, causing their degranulation in a manner that exposes CD107a molecules to the outer side of the membrane.

Here, we imaged the exposed CD107a using fluorescently labeled monoclonal antibody (Fig. 5a and b), and by this way identified which of the cell were activated. Importantly, we did not permeabilized the activated NK cells to prevent the pene-

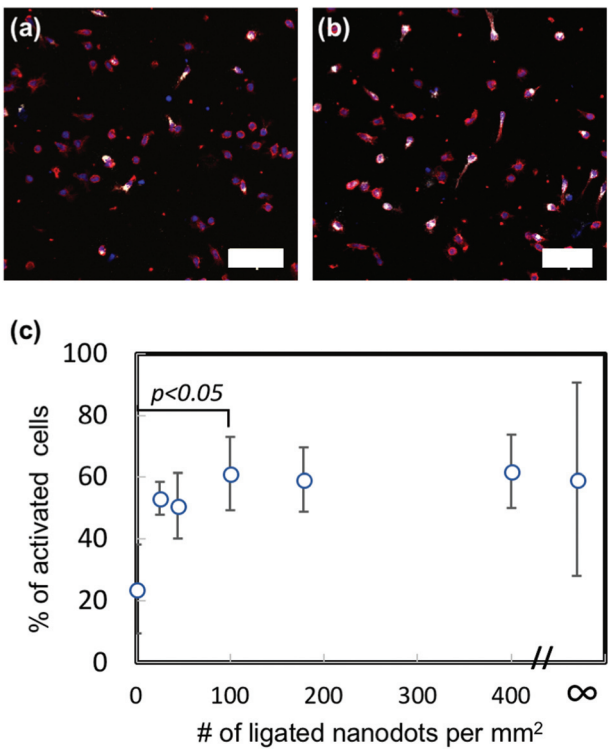

Fig. 5 NK cell activation (a) and (b). Fluorescent imaging of CD107a (white) in the NK cells activated on NK cells activated on the matrices with 400 nanodots per μm^2 and 50 nanodots per μm^2, respectively. The cells were also stained for cytoskeleton (red), nuclei (blue). Scale bars: 50 μm (c) % of activated cells *vs.* the nanodot density. Here ∞ means continues AuPd layer functionalized with MICA, providing the maximal ligand density. Analysis of variance was performed to assess the significant changes in the percentage of activated cells on different matrices. The results were considered significant for $p < 0.05$.

tration of CD107a antibody into the cell cytosol and staining of internal CD107a. To determine which cells were activated and which were not, we defined a threshold for activation, which was the weakest fluorescence intensity of the CD107a that we could observe. Above this value we considered the cells as activated.

Fig. 5c presents the percentage of activated cells after 3 hours of spreading *vs.* the matrix density. The activation percentage of about 30% was observed for the cells spread on the background glass with no presence of MICA molecules. This non-specific cell degranulation can be attributed to mechanical forces generated by the interaction NK cells with poly-L-lysine coated glass.[42–44] The percentage of the activated NK cells increases moderately and nearly linearly with ligand density, for the low densities below 100 dots per square micron. The density of 100 dots per square micron seems, again, to be the threshold, above which most of the cells underwent activation, reaching a maximum percentage of around 60%. This activation percentage is twice higher than that obtained for the NK cells plated on the backgrounds glass surface, and is nearly similar to that obtained for the denser patterns, as well as for plain AuPd surface with the maximal possible surface density of MICA.

Average degranulation per NK cells is not affected by ligand density

To provide a deeper insight into the mechanism by which MICA density affects the cytotoxic activity of NK cells, we monitored the fluorescent intensity of CD107a antibody per individual cell, among the cells considered to be activated (see previous section). Fig. 6 shows the average fluorescent signal of CD107a antibody per cell. The signal here was normalized to the average signal of CD107a collected from a cell that spread on plain AuPd area functionalized with continuous MICA layer. Interestingly, cells plated on different matrices, as well as on the glass background and MICA functionalized AuPd film, produced nearly similar CD107a antibody signal per cell. In other words, we didn't see any pronounced effect of the presence and spatial distribution on MICA ligands on the amount of antigen-induced expression of CD107a on NK cell membrane resulting from degranulation.

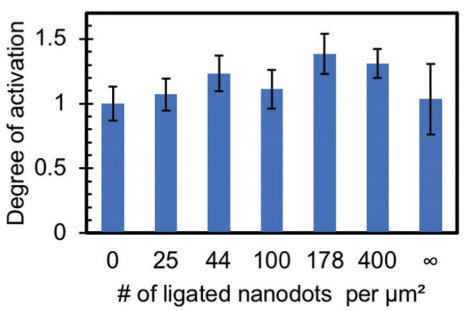

Fig. 6 Average signal of CD107a per activated cell on different areas on the chip.

Discussion

Nanomaterials that controllably mimic bio-interfaces have been extensively used to study function of cells.[45–49] In particular, surfaces patterned with metallic nanoparticles functionalized with ligands have been used to study the effect of spatial ligand distribution on the function of cells such as fibroblasts, stem cells, and T cells.[33–35,50–53] At the same time, the effect of ligand distribution on different NK cell functions, such as spreading, activation of NK receptors, formation of immune synapse with APC, and cytotoxicity, has been barely explored. The ability to investigate the relationship between the spatial distribution of NK ligands and the immune activity of NK cells must rely on the positioning of the ligands in arbitrary chosen geometry, which can precisely regulate the clustering of the activating receptors within the cell membrane. In this work, we presented a robust and facile approach for the functionalization of metallic nanodots with MICA ligands. Our functionalization protocol was based on the selective immobilization of His-conjugated MICA onto AuPd nanodots covered by chemisorbed thiols terminated with chelated NTA. Furthermore, we demonstrated that indirect immunofluorescent staining can be used to verify the selectivity of this biofunctionalization. Indeed, 5-fold difference in the fluorescence signal between the background glass surface and the matrix with the 400 MICA-functionalized nanodots per square micron (the densest array used in this study), indicates that MICA immobilization of the nanodots was very site-specific.

Our novel approach for the immobilization of MICA ligands onto AuPd nanodots, in combination with our previously reported nanoimprint-based fabrication of multiple nanodots matrices, allowed us to engineer a unique nanochip, which contained distinct sectors for NK cell activation through precisely tuned ligand arrangement. Such a chip allows parallel and simultaneous study of the immune response of NK cells to systematically varied activating conditions. Notably, several previous studies employing patterned and ligated nanodots for the spatial control of transmembrane receptors were based on hexagonal nanodots arrays[33,35,53,54] fabricated by self-assembly based lithography.[55] To the best of our knowledge, there has been no clear evidence that transmembrane proteins of any type preferentially cluster in either hexagonal, orthogonal, or any other specific geometry. In this work, we arranged nanodots in an orthogonal matrix, which is viewed by us as the simplest and most basic form to start the investigation of the role of the molecular order of ligand–receptor pairs in NK cell synapse. Further studies should explore additional geometries of NKG2D-MICA arrangement, as well as of other ligand–receptor pairs in cells, to understand whether they preferentially cluster in any specific form. Such studies require a complete freedom of design of the nanodot arrangement, which can be achieved by either electron-beam lithography or nanoimprint lithography. Notably, electron-beam lithography is a serial fabrication technique, and thus is unpractical for scalable fabrication of large-area nanopatterns. On the contrary, nanoimprint lithography combines high patterning resolution and high

throughput, and therefore can be considered as the ultimate approach to produce ligated nanopatterns with freely chosen geometries.

In this work, we elucidated the effect of MICA spatial distribution on the spreading of NK cells, by comparing the average area of cells exposed to different MICA arrays. The observed regulation of the NK cell spreading by the abundancy of available MICA ligands can be viewed through the activation mechanism of NKG2D. NKG2D signals by forming a complex with the short transmembrane molecule DAP10 that includes a tyrosine-based motif (YxxM).[56] Upon its phosphorylation, DAP10 recruits the p85 subunit of phosphoinositide 3-kinase (PI3K), or Grb2 and the effector molecule Vav1 (Grb2-Vav1).[57,58] Activated PI3K binds, in turn, to the small adaptor CrKL, which promotes NKG2D regulated adhesion with the target cell, as well as the migration of granules toward the formed immune synapse, and degranulation. CrKL activates GTPases Rac1 and Rap1 through binding to guanine nucleotide exchange factor, promoting cell adhesion and spreading.[59,60] Here, we not only observed a clear effect of the MICA availability on NK cell spreading, but also the existence of a spreading threshold around 100 ligated nanodots per square micron, below which the cells didn't spread, and above which they spread to the projected area ~3-fold higher than that of non-spread cells. Interestingly, the average projected area was barely varied with the dot density above this threshold.

Further evidence that the spatial distribution of MICA ligands plays a key role in cytotoxic activation of NK cells is based on our degranulation experiments. Indeed, we found that increasing the ligand density led to the increase in the signal produced by CD107a antibody, and that the minimal density of 100 ligated nanodots per square micron is the threshold required for optimal activation.[40] Here, the activation of NKG2D initiates NK cell effector functions, resulting in cytotoxicity facilitated by the release of secretory lysosomes containing perforin and granzymes. While released, secretory lysosomes transfer the lysosome-associated membrane protein CD107a is transported to the surface of the NK cell. Binding CD107a to labeled antibodies enables to detect degranulation of individual NK cells by fluorescent imaging. Notably, we found that the percentage of the activated NK cells plateaus for nanodot densities of 100 ligated nanodots per square micron and above.

Recent studies employing arrays of sub-10 nm metallic nanodots functionalized with cognate ligands for T cell receptors experimentally estimated that each nanodot is occupied on average with 1–1.5 ligands.[53,61] Similarly to these studies, here we used MICA-functionalized sub-10 nm nanodots to spatially control ligand–receptor complexes that are ~ 10 nm in size. Thus, we can assess that the matrix of 100 nanodots per square micron provided between 100 to 150 MICA ligands per square microns available for the recognition by NKG2D receptors. Our results clearly indicated that this range of the ligand density provides the minimal requirement for NK cell activation and spreading. The fact that both spreading and activation showed similar dependence on the ligand spatial distribution, including the 100 dots/square micron threshold and the post threshold plateau, is not surprising. As mentioned above, NKG2D mediated activation followed by degranulation promotes spreading.[59,60] Our findings, therefore, confirms that spreading and MICA regulated activation are two closely related processes in NK cells, which most likely depend on the environmental factors in similar manner.

Interestingly, whereas the abundancy and spatial distribution of activating ligands affected the overall amount of activated NK cells, it did not influence the average quantity of the detected CD107a per individual activated cell. In other words, while the availability and density of MICA has an effect on the probability of a NK cell to be activated, it barely correlates with the amount of vesicles released by each activated NK cell. This finding reflects the notion that when the antigen amount is above the threshold, all NK cells release the nearly constant load of lytic vesicles, which in turn leads to the same amount of CD107a molecules located at the cell membrane.[62,63] In other words, we observed on–off behavior of NK immune response, which was obtainable because our quantitative method allowed us to decipher between the percentage and degree of activation. A certain quantity of activated NK cells found on the glass background areas can be interpreted through the possible self-activation in the absence of activating ligands. In addition, the activation NK cells on glass background can be facilitated by non-specific immobilization of MICA ligands on glass.

The regulation of the activation of immune cells by the nano-spacing of activating ligands has been attracting a great deal of interest in the nano-research and immunology community. Recently, Delcassian *et al.* reported on the correlation between nanoscale spacing of nanopatterned dots functionalized with anti-CD3 ligands and the extent of membrane-localized phosphotyrosine produced by effector T cells.[35] Similarly, Deeg *et al.* recently showed a correlation between the nanoscale spacing of nanopatterned dots functionalized with pMHC and the amount of secreted interleukin-2 (IL-2).[53] Notably, here we focused on NK cells, and used different activation markers from those used by previous studies. Therefore, certain differences in how the ligand arrangement mediates the marker secretion are possible. Furthermore, in the previous studies, a cumulative signal of the secreted activation markers was collected from the colonies of multiple cells. Thus, the observed variations in the marker quantity between different ligand arrays might stem from the fact that either (i) denser ligand arrays stimulated a higher average amount of the secreted marker per cell, or (ii) denser ligand arrays activated a higher percentage of cells. Here, we separately assessed the percentage of activated cells and the average the amount of the marker secreted by individual cells, and concluded that the second scenario is more likely relevant in our case.

In summary, we studied how NKG2D antigens regulate spreading and activation of NK cells. This study was possible by using biochip with multiple isolated microenvironments for immune activation of NK cell. These microenvironments

regulate spatial distribution of ligands with molecular resolution. Our study provided an important insight on the spatial mechanism of the cytotoxic activity of NK cells. In particular, it established that ligand distribution within the 100 nm length-scale is a critical barrier for the NK cell activation and degranulation. Importantly, the cytotoxicity of NK cells is regulated by the subtle balance of multiple activating, costimulatory, and inhibitory receptors. Clearly, to understand how NK cells coordinate and integrate different signaling inputs, the exact individual role of each of the receptors participating in this process must be deciphered as well as in combination with other receptors. Future investigations should be directed to creating a platform that controllably integrates NKG2D signaling with the signals of other receptors, enabling a more comprehensive understanding of the complexity and diversity of NK immune synapse. This understanding will pave the way to rationally designed immunotherapeutic approaches employing the unique NK cytotoxicity against human malignancies.

Ethical statement

Human Natural Killer cells were purified from peripheral blood of healthy, adult, volunteer donors, recruited by written informed consent, as approved by the Institutional Review Board Ben-Gurion University of the Negev (BGU) in accordance with the Declaration of Helsinki.

Conflicts of interest

The authors have no conflicts to declare.

Acknowledgements

This work was funded by the Multidisciplinary Research Grant – The Faculty of Health Science in Ben-Gurion University of the Negev, Israel Ministry of Science and Technology: Israel-Taiwan Collaborative Grant # 3-12409, and Israel Science Foundations: F.I.R.S.T. Individual Grant # 2058/18. The manuscript was written through contributions from all authors.

References

1 R. Herberman, M. E. Nunn and D. H. Lavrin, *Int. J. Cancer*, 1975, **16**, 216–229.
2 R. Kiessling, E. Klein, H. Pross and H. Wigzell, *Eur. J. Immunol.*, 1975, **5**, 117–121.
3 M. J. Smyth, Y. Hayakawa, K. Takeda and H. Yagita, *Nat. Rev. Cancer*, 2002, **2**, 850–861.
4 J. S. Orange, *J. Allergy Clin. Immunol.*, 2013, **132**, 515–525.
5 J. F. Bukowski, B. Woda and R. M. Welsh, *J. Virol.*, 1984, **52**, 119–128.
6 H. G. Ljunggren and K. Karre, *Immunol. Today*, 1990, **11**, 237–244.
7 J. Westermann and R. Pabst, *Clin. Invest.*, 1992, **70**, 539–544.
8 D. M. Baume, M. J. Robertson, H. Levine, T. J. Manley, P. W. Schow and J. Ritz, *Eur. J. Immunol.*, 1992, **22**, 1–6.
9 J. S. Orange, *Nat. Rev. Immunol.*, 2008, **8**, 713–725.
10 D. M. Davis, I. Chiu, M. Fassett, G. B. Cohen, O. Mandelboim and J. L. Strominger, *Proc. Natl. Acad. Sci. U. S. A.*, 1999, **96**, 15062–15067.
11 N. Guerra, Y. X. Tan, N. T. Joncker, A. Choy, F. Gallardo, N. Xiong, S. Knoblaugh, D. Cado, N. R. Greenberg and D. H. Raulet, *Immunity*, 2008, **28**, 571–580.
12 S. Bauer, *Science*, 1999, **285**, 727–729.
13 N. T. Joncker, N. Shifrin, F. Delebecque and D. H. Raulet, *J. Exp. Med.*, 2010, **207**, 2065–2072.
14 D. H. Raulet, *Nat. Rev. Immunol.*, 2003, **3**, 781–790.
15 P. Obeidy and A. F. Sharland, *Int. J. Biochem. Cell Biol.*, 2009, **41**, 2364–2367.
16 J. Zhang, F. Basher and J. D. Wu, *Front. Immunol.*, 2015, **6**, 1–7.
17 D. Pende, P. Rivera, S. Marcenaro, C.-C. Chang, R. Biassoni, R. Conte, M. Kubin, D. Cosman, S. Ferrone, L. Moretta and A. Moretta, *Cancer Res.*, 2002, **62**, 6178–6186.
18 H. R. Salih, H.-G. Rammensee and A. Steinle, *J. Immunol.*, 2002, **169**, 4098–4102.
19 V. Groh, J. Wu, C. Yee and T. Spies, *Nature*, 2002, **419**, 734–738.
20 D. Cosman, J. Müllberg, C. L. Sutherland, W. Chin, R. Armitage, W. Fanslow, M. Kubin and N. J. Chalupny, *Immunity*, 2001, **14**, 123–133.
21 R. A. Eagle, J. A. Traherne, O. Ashiru, M. R. Wills and J. Trowsdale, *Hum. Immunol.*, 2006, **67**, 159–169.
22 V. Tieng, C. Le Bouguénec, L. du Merle, P. Bertheau, P. Desreumaux, A. Janin, D. Charron and A. Toubert, *Proc. Natl. Acad. Sci. U. S. A.*, 2002, **99**, 2977–2982.
23 V. Groh, R. Rhinehart, J. Randolph-Habecker, M. S. Topp, S. R. Riddell and T. Spies, *Nat. Immunol.*, 2001, **2**, 255–260.
24 M. Jinushi, T. Takehara, T. Kanto, T. Tatsumi, V. Groh, T. Spies, T. Miyagi, T. Suzuki, Y. Sasaki and N. Hayashi, *J. Immunol.*, 2003, **170**, 1249–1256.
25 S. Nedvetzki, S. Sowinski, R. A. Eagle, J. Harris, F. Vély, D. Pende, J. Trowsdale, E. Vivier, S. Gordon and D. M. Davis, *Blood*, 2007, **109**, 3776–3785.
26 V. Groh, S. Bahram, S. Bauer, A. Herman, M. Beauchamp and T. Spies, *Proc. Natl. Acad. Sci. U. S. A.*, 1996, **93**, 12445–12450.
27 H. Ghadially, L. Brown, C. Lloyd, L. Lewis, A. Lewis, J. Dillon, R. Sainson, J. Jovanovic, N. J. Tigue, D. Bannister, L. Bamber, V. Valge-Archer and R. W. Wilkinson, *Br. J. Cancer*, 2017, **116**, 1208–1217.
28 Y. T. Bryceson, H. G. Ljunggren and E. O. Long, *Blood*, 2009, **114**, 2657–2666.
29 L. Martinet and M. J. Smyth, *Nat. Rev. Immunol.*, 2015, **15**, 243–254.

30 E. O. Long, H. Sik Kim, D. Liu, M. E. Peterson and S. Rajagopalan, *Annu. Rev. Immunol.*, 2013, **31**, 227–258.
31 L. L. Lanier, *Nat. Immunol.*, 2008, **9**, 495–502.
32 P. Li, D. L. Morris, B. E. Willcox, A. Steinle, T. Spies and R. K. Strong, *Nat. Immunol.*, 2001, **2**, 443–451.
33 M. Arnold, E. A. Cavalcanti-Adam, R. Glass, J. Blümmel, W. Eck, M. Kantlehner, H. Kessler and J. P. Spatz, *ChemPhysChem*, 2004, **5**, 383–388.
34 M. Schvartzman, M. Palma, J. Sable, J. Abramson, X. Hu, M. P. Sheetz and S. J. Wind, *Nano Lett.*, 2011, **11**, 1306–1312.
35 D. Delcassian, D. Depoil, D. Rudnicka, M. Liu, D. M. Davis, M. L. Dustin and I. E. Dunlop, *Nano Lett.*, 2013, **13**, 5608–5614.
36 M. Schvartzman and S. J. Wind, *Nano Lett.*, 2009, **9**, 3629–3634.
37 S. V. Pageon, S.-P. Cordoba, D. M. Owen, S. M. Rothery, A. Oszmiana and D. M. Davis, *Sci. Signaling*, 2013, **6**, 62.
38 G. Le Saux, A. Edri, Y. Keydar, U. Hadad, A. Porgador and M. Schvartzman, *ACS Appl. Mater. Interfaces*, 2018, **10**, 11486–11494.
39 B. Rosental, M. Brusilovsky, U. Hadad, D. Oz, M. Y. Appel, F. Afergan, R. Yossef, L. A. Rosenberg, A. Aharoni, A. Cerwenka, K. S. Campbell, A. Braiman and A. Porgador, *J. Immunol.*, 2011, **187**, 5693–5702.
40 G. Alter, J. M. Malenfant and M. Altfeld, *J. Immunol. Methods*, 2004, **294**, 15–22.
41 E. Aktas, U. C. Kucuksezer, S. Bilgic, G. Erten and G. Deniz, *Cell. Immunol.*, 2009, **254**, 149–154.
42 G. Giannone and M. P. Sheetz, *Trends Cell Biol.*, 2006, **16**, 213–223.
43 C. C. Gross, J. A. Brzostowski, D. Liu and E. O. Long, *J. Immunol.*, 2010, **185**, 2918–2926.
44 R. Basu, B. M. Whitlock, J. Husson, A. Le Floc'h, W. Jin, A. Oyler-Yaniv, F. Dotiwala, G. Giannone, C. Hivroz, N. Biais, J. Lieberman, L. C. Kam and M. Huse, *Cell*, 2016, **165**, 100–110.
45 L. Zhang and T. J. Webster, *Nano Today*, 2009, **4**, 66–80.
46 P. Cai, M. Layani, W. R. Leow, S. Amini, Z. Liu, D. Qi, B. Hu, Y. L. Wu, A. Miserez, S. Magdassi and X. Chen, *Adv. Mater.*, 2016, **28**, 3102–3110.
47 B. Hu, W. Shi, Y. L. Wu, W. R. Leow, P. Cai, S. Li and X. Chen, *Adv. Mater.*, 2014, **26**, 5786–5793.
48 B. Hu, W. R. Leow, S. Amini, B. Nai, X. Zhang, Z. Liu, P. Cai, Z. Li, Y. L. Wu, A. Miserez, C. T. Lim and X. Chen, *Adv. Mater.*, 2017, **29**, 1700145–1700155.
49 M. A. Dobrovolskaia and S. E. McNeil, *Nat. Nanotechnol.*, 2007, **2**, 469–478.
50 X. Wang, S. Li, C. Yan, P. Liu and J. Ding, *Nano Lett.*, 2015, **15**, 1457–1467.
51 M. Schvartzman, K. Nguyen, M. Palma, J. Abramson, J. Sable, J. Hone, M. P. Sheetz and S. J. Wind, *J. Vac. Sci. Technol., B: Nanotechnol. Microelectron.: Mater., Process., Meas., Phenom.*, 2009, **27**, 61.
52 H. Cai, D. Depoil, M. Palma, M. P. Sheetz, M. L. Dustin and S. J. Wind, *J. Vac. Sci. Technol., B: Nanotechnol. Microelectron.: Mater., Process., Meas., Phenom.*, 2013, **31**, 06F902.
53 J. Deeg, M. Axmann, J. Matic, A. Liapis, D. Depoil, J. Afrose, S. Curado, M. L. Dustin and J. P. Spatz, *Nano Lett.*, 2013, **13**, 5619–5626.
54 E. A. Cavalcanti-Adam, A. Micoulet, J. Blümmel, J. Auernheimer, H. Kessler and J. P. Spatz, *Eur. J. Cell Biol.*, 2006, **85**, 219–224.
55 R. Glass, M. Muller and J. P. Spatz, *Nanotechnology*, 2003, **14**, 1153–1160.
56 J. Wu, Y. Song, A. B. H. Bakker, S. Bauer, T. Spies, L. L. Lanier and J. H. Phillips, *Science*, 1999, **285**, 730–732.
57 J. L. Upshaw, L. N. Arneson, R. A. Schoon, C. J. Dick, D. D. Billadeau and P. J. Leibson, *Nat. Immunol.*, 2006, **7**, 524–532.
58 S. Gilfillan, E. L. Ho, M. Cella, W. M. Yokohama and M. Colonna, *Nat. Immunol.*, 2002, **3**, 1150–1155.
59 W. T. Arthur, L. A. Quilliam and J. A. Cooper, *J. Cell Biol.*, 2004, **167**, 111–122.
60 W.-J. Pannekoek, M. R. H. Kooistra, F. J. T. Zwartkruis and J. L. Bos, *Biochim. Biophys. Acta*, 2009, **1788**, 790–796.
61 H. Cai, H. Wolfenson, D. Depoil, M. L. Dustin, M. P. Sheetz and S. J. Wind, *ACS Nano*, 2016, **10**, 4173–4183.
62 N. J. Topham and E. W. Hewitt, *Immunology*, 2009, **128**, 7–15.
63 Y. T. Bryceson, M. E. March, D. F. Barber, H.-G. Ljunggren and E. O. Long, *J. Exp. Med.*, 2005, **202**, 1001–1012.